Dynamics of Extreme Nonequilibrium Electron Transport in GaAs

J. R. HAYES AND A. F. J. LEVI
(*Invited Paper*)

Abstract—**Hot electron effects have been observed in semiconductors for many decades; however, until recently, direct experimentally determined spectroscopic information on the hot electron distribution function did not exist. As a result the microscopic basis for hot electron transport could only be inferred. To bridge the gap between theory and experiment we invented *hot electron spectroscopy*, a technique which enabled us to obtain direct spectroscopic information on the electron momentum distribution, $n(p)$. In this paper we describe the technique and discuss hot electron spectra obtained in GaAs. "Ballistic" electron transport is observed in samples having narrow transit regions (<850 Å) and near diffusive transport for samples having wide transit regions (>1700 Å). In addition, a theoretical model has been developed enabling us to identify all observed features in the spectra.**

IN the early 1960's considerable effort was directed toward the development of metal base hot and "ballistic" electron transistors for high-speed device applications. However, materials problems, quantum mechanical reflection from abrupt interfaces, and strong electron scattering limited the performance of these devices to common emitter current gains of less than unity [1]. With such severe limitations high-performance electronic devices of this type could not readily be achieved and interest in their development declined.

With the continuing advance of semiconductor processing technology Shannon was able to realize a hot electron transistor (HET) in silicon [2]. The energy band diagram for such a device is shown in Fig. 1(a) having a camel diode collector and a Schottky barrier as the emitter. The high capacitance of the Schottky barrier emitter led Shannon to propose a second HET structure replacing the Schottky barrier with a camel diode [see Fig. 1(b)] thereby creating an all semiconductor transistor [3]. These structures were, however, fabricated by ion implantation which did not allow atomic scale control of doping profiles. A bulk triangular barrier structure similar to that of the camel diode, but using the precise doping profiles obtainable by molecular beam epitaxy (MBE), was demonstrated by Malik *et al.* [4]. They termed their structure a "planar doped barrier" and by placing two of them back to back they fabricated the first HET in GaAs [5].

Thus, the advent of thin film epitaxial crystal growth techniques led to a resurgence of interest in the "ballistic electron transistor" (BET). Epitaxial crystal growth of the semiconductor alloy system GaAs/GaAlAs is sufficiently well characterized that one may grow single crystal layers of almost arbitrary composition and carrier concentration. This unique degree of control allows one to translate metal-oxide-metal tunnel junctions into GaAs/AlGaAs/GaAs tunnel junctions and metal-semiconductor Schottky barriers into either GaAs/AlGaAs heterojunctions, camel diodes or planar doped barriers. In this sense the "ballistic" transistor concepts of the early 1960's are beginning to find their semiconductor analogues today with particular interest being shown in the development of a BET in the GaAs/AlGaAs material system [6].

In addition to such transistors being of significant technological interest they also provide an unique opportunity to study the physics of hot electron transport in semiconductors. There have been many reports of hot electron

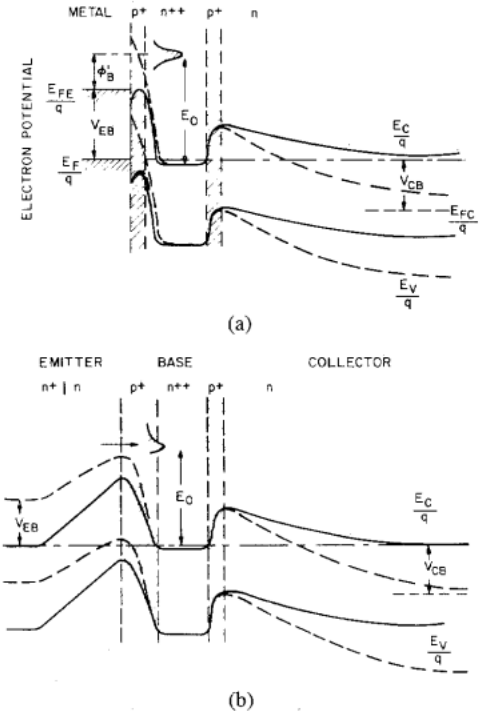

Fig. 1. Schematic energy band diagram for two HET's made by Shannon. (a) HET with Schottky emitter. (b) HET with camel emitter. The solid line represents the unbiased structure whilst the broken line shows it biased with respect to the base. Shannon's hot electron transistor. Reproduced with permission of IEE.

Manuscript received April 15, 1986; revised April 23, 1986.

J. R. Hayes is with Bell Communications Research, Murray Hill, NJ 07974.

A. F. J. Levi is with AT&T Bell Laboratories, Murray Hill, NJ 07974.

IEEE Log Number 8609657.

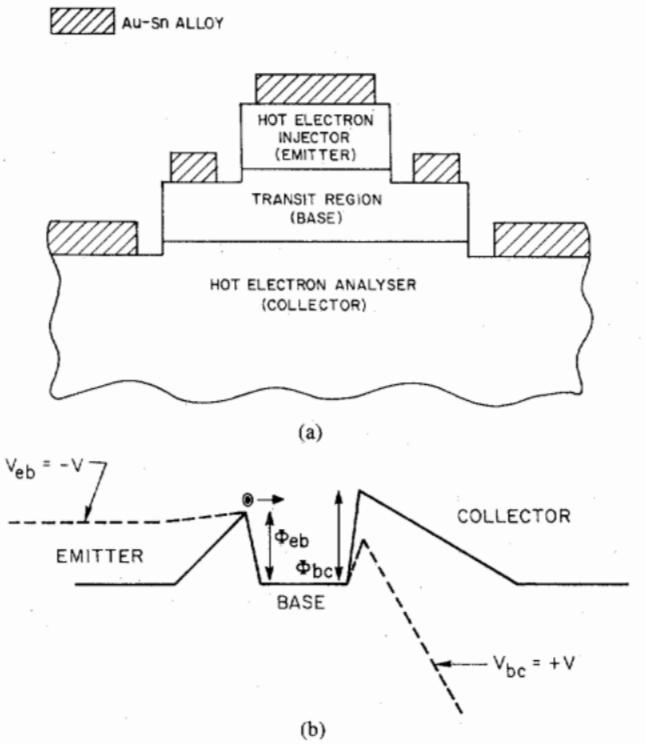

Fig. 2. (a) Schematic diagram of the MBE grown GaAs epilayers comprising the two level mesa structure. (b) Schematic diagram of the conduction band edge of a hot electron injector (emitter), transit region (base) and hot electron analyzer (collector). Typically, the long and short arms of the triangular barriers have an aspect ratio of 10 with a short arm width of 150 Å. The broken line indicates the conduction band edge of the structure when biased.

effects in semiconductors in the past. Some notable events have been the observation of saturation in the velocity-field characteristic of germanium reported by Schockley and Ryder [7], the measurement of a negative differential resistance in GaAs by Gunn [8] and the observation of hot carrier luminescence by Shah and Leite [9]. However, none of these measurements gave direct spectroscopic information on the hot electron momentum distribution function, $n(p)$. Consequently, until recently, the predictions of theorists had never been subject to a meaningful empirical test namely comparison with an experimentally observed distribution function. This situation changed with our invention of a technique called "hot electron spectroscopy" in which direct information on hot electron distribution functions in semiconductors could be obtained [10], [11].

The results described in this paper were obtained by means of a planar GaAs structure, a schematic diagram of which is shown in Fig. 2. The structure was grown by MBE at 650°C on a ⟨100⟩-orientated semi-insulating GaAs substrate with use of cracked As_4. After growth of a thick n^+ (Si impurity) buffer layer two separate bulk triangular potential barriers were formed. Each potential barrier was made by placement of an approximately 100 Å thick p^+ (Be impurity) layer in a region of low carrier concentration ($< 1 \times 10^{15}$ cm^{-3}) bounded on either side by n^+ layers. The wafers were fabricated into two-level mesa structures in order that the three n^+ regions could be contacted individually [see Fig. 2(a)]. The first etch, which has a critical depth dependence, was achieved by the successive growth and removal of an anodic oxide grown in $H_2O:H_3PO_4$ having a Ph of 2.5. The third n^+ region, to which the collector contact was made, was revealed using a standard $100H_2O:10H_3PO_4:2H_2O_2$ chemical etch. Ohmic contacts were formed by rapidly thermally annealing an evaporated Au–Sn alloy.

A schematic diagram of the energy band structure used for hot electron spectroscopy is shown in Fig. 2(b). Electrical contact is made to three n-type degenerately doped GaAs regions which are separated by two bulk triangular barriers. Since the structure resembles a unipolar transistor, we use standard transistor notation to describe the currents and voltages involved. The emitter-base junction functioned as a hot-electron injector and the base-collector junction as a hot-electron analyzer. Between the hot-electron injector and analyzer was a short n^+ transit region, analogous to the base of a unipolar transistor where electron scattering took place. Typically the triangular potential barriers, which form the injector (emitter) and analyzer (collector), were fabricated such that the electron injection energy E_i was lower than the unbiased analyzer barrier energy ϕ_{bc}. Both triangular barriers had an aspect ratio of approximately 10 with the shorter arm of each adjoining the n^+ transit region and being 150 Å thick. The short arm's impurity concentration and small thickness ensured that their contribution to electron scattering was insignificant. All electrical measurements were made with respect to a grounded base.

When the emitter was biased negative electrons were injected into the base region with an excess energy ($\phi_{eb} - E_F$) above the Fermi energy E_F. With a small positive bias on the collector no electrons were collected as none had sufficient energy to traverse the collector barrier ϕ_{bc}. With increasing base-collector bias, the barrier, ϕ_{bc} is decreased, as indicated by the broken lines in Fig. 2. Hence, a means for continuous variation of the base-collector barrier energy was established, which enabled spectroscopic information about the current arriving at the analyzer barrier to be obtained. At a given base-collector bias V_{bc} the collector current flow I_c is proportional to the fraction of the injected electrons able to traverse the base-collector barrier. An outline of the factors determining I_c is given below.

Consider first electrons injected into the base from the emitter. Electrons can only be injected if, at the top of the barrier, they have a component of momentum in the direction of the base. For those electrons injected into the base, the component of momentum parallel to the emitter plane ($p_\parallel$) is conserved, whereas the component of momentum normal to the emitter plane ($p_\perp$) is dramatically increased. Hence a maximum angle exists for electron injection (θ_{max}) that is given by

$$\theta_{max} = \tan (p_\parallel / p_\perp). \quad (1)$$

Given the assumption of a parabolic conduction band, an

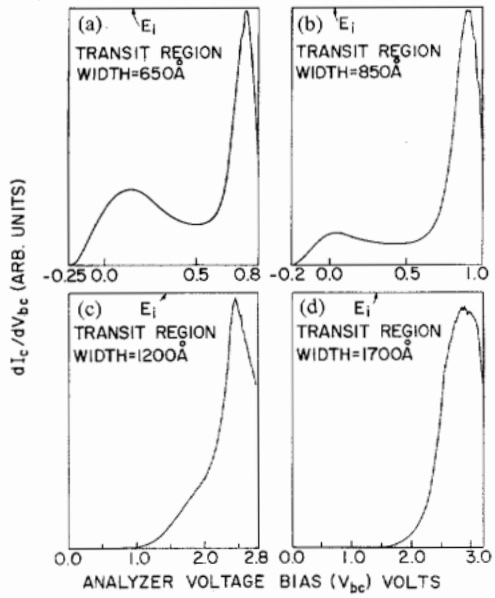

Fig. 3. Measured hot electron spectra of four samples differing in transit region width. (a) 650 Å. (b) 850 Å. (c) 1200 Å. (d) 1700 Å. The injection energy E_i is indicated in each spectrum. The Fermi energy is to the extreme right of each plot.

electron injected into the base at 0.25 eV would have a $\theta_{\max}$ of much less than 10° at low temperatures (~4.2 K).

Electrons injected into the base suffer elastic and inelastic collisions, which cause significant energy loss and angular scattering. Hence, hot electrons arriving at the analyzer barrier may be described in terms of a distribution of possible $p_\perp$ values $n(p_\perp)$ such that the total current flow, I_c for a given barrier energy ϕ_{bc} is

$$I_c = -(e/m_e^*) \int_{p_\perp^0}^{\infty} p_\perp n(p_\perp)\, dp_\perp \tag{2}$$

where m_e^* is the effective electron mass, e the electronic charge, and $p_\perp^0 = (2m_e^*\phi_{bc})^{1/2}$.

Taking the derivative of I_c in (2) with respect to V_{bc} gives [11]

$$\frac{dI_c}{dV_{bc}} = \frac{e}{m_e^*}\frac{d\phi_{bc}}{dV_{bc}}\frac{dp_\perp^0}{d\phi_{bc}} n(p_\perp^0)p_\perp^0. \tag{3}$$

Equation (6) of Kazarinov and Luryi [12] shows that V_{bc} is related linearly to ϕ_{bc}, i.e., the analyzer energy varies linearly with bias. It then follows that

$$\frac{dI_c}{dV_{bc}} \propto n(p_\perp^0). \tag{4}$$

Hence, by differentiating I_c with respect to V_{bc} we may obtain the electron momentum distribution at the base-collector junction [11].

Four spectra measured at 4.2 K to eliminate thermal smearing effects, are presented in Fig. 3. The spectra were obtained from samples having similar hot electron injection energies ($E_i \cong 0.25$ eV) and the same n-type doping level of 1×10^{18} cm^{-3} in the transit region; samples differed in transit region width. Fig. 3 shows spectra of samples having transit region widths (a) 650 Å, (b) 850 Å, (c) 1200 Å, and (d) 1700 Å. As may be seen there is a dramatic change in the hot electron spectra with small changes in transit region width, indicative of strong scattering. The hot electron spectra always show a characteristic peak close to the Fermi energy E_F. Only in the samples having narrow transit region widths [Fig. 3(a) and (b)] is there pronounced evidence of the initial injected distribution, i.e., "ballistic" electrons. The observation of "ballistic" electron transport was first presented by us in an invited presentation at the 1985 March meeting of the American Physical Society and subsiquently published in *Physical Review Letters* [13]. This observation was later confirmed by Heiblum *et al.* [14] using a differently designed spectrometer. Unfortunately, a complete hot electron spectrum was not obtained, so that experimental results at low-analyzer barrier energies could not be compared.

To understand the electron scattering mechanisms giving rise to the hot electron spectra shown in Fig. 3 we have developed a theory of nonequilibrium electron transport [13], [15]. In intrinsic or very lightly doped GaAs, hot electrons with energies greater than the longitudinal optical (LO) phonon energy, are inelastically scattered by the emission of LO phonons. However, at carrier concentrations of $\sim 1 \times 10^{18}$ cm^{-3} the long wavelength collective oscillatory (plasmon) mode of the n^+ electron gas is close in energy to that of the LO phonons. These two longitudinal oscillations do not exist independently of each other but interact strongly creating a coupled plasmon/phonon system. It is, therefore, physically incorrect to describe hot electron scattering in terms of separate contributions from phonon and plasmon modes in n^+GaAs [16]. In addition to hot electrons being inelastically scattered from long wavelength coupled plasmon/phonon collective modes, they may also scatter via the creation of single electron-hole pairs (the so-called electron-hole continuum). With decreasing wavelength the collective modes are damped by the continuum leaving only the continuum and optical phonons contributing to the scattering.

We first consider the problem of scattering a hot electron from a thin "sample" of doped GaAs. If the nonequilibrium electrons are of sufficient energy and the probability of electrons scattering from our "sample" is small then we may use the Born approximation to calculate the scattering. For a thick sample in which multiple scattering must be taken into account then a more complicated Monte Carlo calculation or some other procedure must be adopted. In this paper we consider the low temperature limit of the simple case first. An electron of energy E_i above the conduction band minimum and wavevector k_i is injected into a thin transit region of doped GaAs. The injected electron acts as a time varying test charge which interacts with the electron/phonon system in the transit region. Perturbation theory may then be applied to obtain the probability that the injected electron loses energy $\hbar\omega$ and is scattered by wavevector, q. These dissipative processes are described by the imaginary part of the dielectric response function of the electron/phonon

system so that the inelastic differential scattering rate is given by [17]

$$dR_{\text{inelastic}} = \frac{8\pi e^2}{\hbar q^2} S(q, \omega) \frac{d^3q}{(2\pi)^3} \tag{5}$$

where $S(q, \omega)$ is the loss function

$$S(q, \omega) = -\text{Im} \frac{1}{\epsilon(q, \omega)}. \tag{6}$$

The frequency and wavevector dependent dielectric function $\epsilon(q, \omega)$, which describes the response of the electron/phonon system to the test charge, may be written as

$$\epsilon(q, \omega) = \epsilon_\infty \left(\frac{\omega^2 - \omega_{LO}^2}{\omega^2 - \omega_{TO}^2}\right) + \chi(q, \omega) \tag{7}$$

in which ω_{LO} and ω_{TO} are the longitudinal and transverse optical phonon frequencies and ϵ_∞ is the high-frequency dielectric constant. The first term in (7) is the long wavelength phonon contribution and the second term, $\chi(q, \omega)$ comes from the conduction electrons. The justification for using the long wavelength limit for the phonons arises from the fact that its dielectric function varies on the scale of the reciprocal lattice vector k_L and in our case the momentum change q for inelastically scattered electrons is such that $q << k_L$.

In general the response of the electrons $\chi(q, \omega)$ cannot be calculated exactly. However, in the limit of high electron carrier concentrations in the transit region (typically $n = 1 \times 10^{18}$ cm^{-3}) the Coulomb interactions among electrons are weak. This is characterized by the r_s value which for $n = 1 \times 10^{18}$ cm^{-3} is less than unity, i.e., $r_s \equiv (\frac{3}{4}\pi n)^{1/3} (m_e^* e^2/\hbar^2 \epsilon_\infty) \cong 0.7$ where $m_e^* = 0.07 m_0$ so that $\chi(q, \omega)$ may be replaced with the familiar noninteracting Lindhard form, $\chi_0(q, \omega)$ where

$$\chi_0(q, \omega) = \frac{\xi}{x^2}\left(2x + \left(1 - 1/4\left(x - \frac{y}{x}\right)^2\right) \cdot \ln\left\{\frac{y - x(x+2)}{y - x(x-2)}\right\} + \left(1 - 1/4\left(x + \frac{y}{x}\right)^2\right) \cdot \ln\left\{\frac{-y - x(x+2)}{-y - x(x-2)}\right\}\right) \tag{8}$$

in which $\xi = m_e^*/2\,(e/\pi\hbar)^2\,(8\pi/3n)^{1/3}$, $x = q/k_F$ and $y = \hbar\omega/E_F$ where k_F is the Fermi wavevector and E_F the Fermi energy.

Substituting (8) into (7) gives the dielectric response $\epsilon(q, \omega) = \epsilon_1(q, \omega) + i\epsilon_2(q, \omega)$ of the coupled electron/phonon system in the transit region. In Fig. 4(a) we plot the real (ϵ_1) and imaginary (ϵ_2) parts of ϵ for a fixed value of $q = 0.1 \times k_F$ as a function of energy loss $\hbar\omega$ for a carrier concentration $n = 1 \times 10^{18}$ cm^{-3}. As may be seen ϵ_1 crosses zero at a number of energies and ϵ_2 has a finite positive value in two energy ranges. In Fig. 4(b) we plot the loss function $S(q, \omega)$ over the same energy range. At low energies (0.0 meV → 12.0 meV) there is a small,

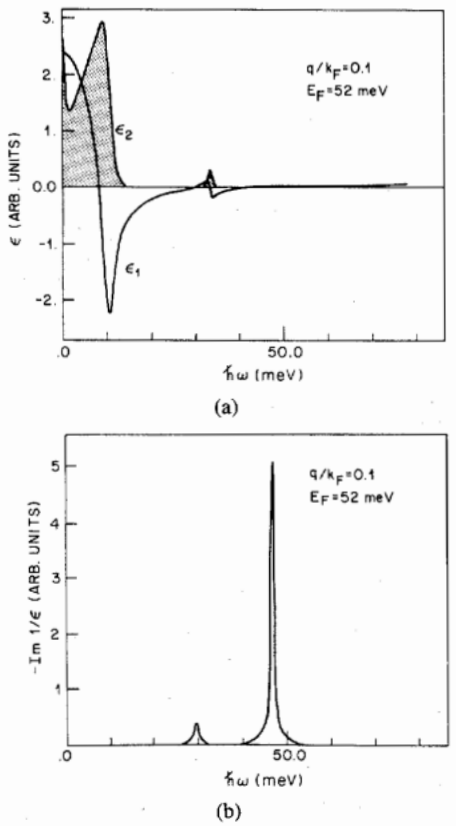

Fig. 4. (a) Plot of the real ϵ_1 and imaginary ϵ_2 part of the dielectric response function, ϵ for a fixed value of $q = 0.1 \times k_F$ as a function of energy loss $\hbar\omega$ at a carrier concentration of 1×10^{18} cm^{-3}. (b) The corresponding loss function for (a).

slowly varying contribution to $S(q, \omega)$ (not shown in the figure) arising from the large value of ϵ_2 in this range. This loss mechanism corresponds to the excitation of single electron hole pairs from the Fermi sea (the so-called electron-hole continuum). The two zero crossings of ϵ_1 at around 30 meV and 45 meV shown in Fig. 4(a) give rise to the two peaks in $S(q, \omega)$ shown in Fig. 4(b) and correspond to long-wavelength, collective, longitudinal excitations of the coupled electron/phonon system.

Information on $S(q, \omega)$ as a function of energy loss $\hbar\omega$ for all scattered wavevectors q is given by the dispersion relation shown in Fig. 5. Here $\hbar\omega$ is shown as a function of q for GaAs having a carrier concentration $n = 1 \times 10^{18}$ cm^{-3}. Because, for this high value of n, both the bare plasmon and optical phonon frequencies are similar they interact to form two coupled plasmon/phonon modes of frequency ω^+ and ω^- at $q = 0$. With increasing wavevector these modes exhibit dispersion and at some modest wavevector ($q/k_F \cong 0.3$) they enter the electron-hole continuum shown by the shaded region. Here the collective plasmon/phonon modes are Landau damped (broken lines in Fig. 5) by the excitation of single electron hole pairs from the Fermi sea. In any given inelastic scattering event there will be a contribution from the coupled plasmon/phonon modes and from the continuum. At larger wavevectors only the dispersionless longitudinal optical phonon mode and the single particle continuum exist.

The function $S(q, \omega)$ which describes the loss processes

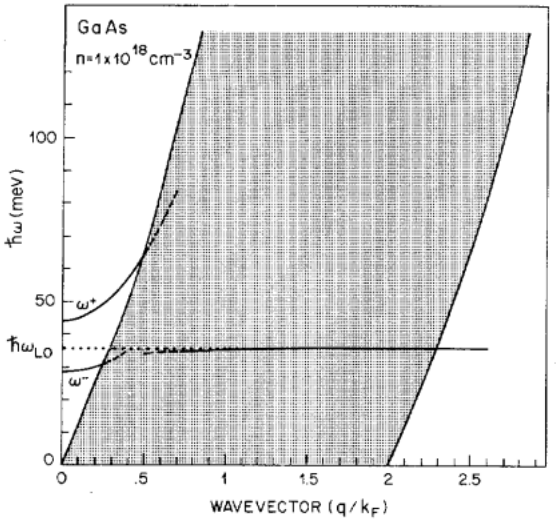

Fig. 5. Dispersion relation for the coupled electron/phonon for GaAs at a carrier concentration $n = 1 \times 10^{18}$ cm^{-3}.

may now be used to obtain a total inelastic scattering rate, $1/\tau_{\text{in}}$, for the incident nonequilibrium electrons of energy E_i. This is achieved by integrating (5) over all q consistent with momentum and energy conservation

$$\frac{1}{\tau_{\text{in}}} = \frac{2m_e^* e^2}{k_i \pi \hbar^2} \int S(q, \omega) \frac{dq}{q} d\omega. \tag{9}$$

The Pauli exclusion principle is included in the calculation by preventing electrons from being scattered into states below the Fermi energy E_F. The loss of energy of nonequilibrium electrons to the coupled electron-phonon system in GaAs is described by (9). Ultimately this energy is dissipated as heat in the sample, but in the linear regime, were the experiments were performed, the details of this process are unimportant. In Fig. 6(a) we plot the calculated total inelastic scattering rate $1/\tau_{\text{in}}$ as a function of E_i, the initial electron energy above the conduction band minimum for GaAs, for several carrier densities. We note that $1/\tau_{\text{in}}$ has not been weighted with energy loss. The scattering rates are, due to the Pauli exclusion principle, zero below E_F for a finite carrier concentration and zero below the longitudinal optical phonon energy ($\hbar\omega_{LO}$) for $n = 0$. For $n = 1 \times 10^{18}$ cm^{-3}, which is relevant for our data, the inelastic scattering rate increases slowly from zero at the Fermi energy $E_F \sim 50$ meV, reaching a maximum of $\sim 2 \times 10^{13}$ s^{-1} at 0.15 eV above the conduction band minimum and remaining essentially constant up to 0.3 eV. Hot electron injection energies greater than 0.3 eV are not considered in the calculation since for energies greater than this other details, such as the change in the character of the electron's wavefunction and the possibility of intervalley scattering, must be taken into account.

For impurity concentrations as high as $n_i = 1 \times 10^{18}$ cm^{-3} in the transit region the role of elastic scattering from ionized impurities must also be considered. Elastic scattering is specified by momentum transfer $q = 2k_i \sin(\theta/2)$ where θ is the scattering angle. In the Born approximation, the total elastic scattering rate, $1/\tau_{\text{el}}$, is given by

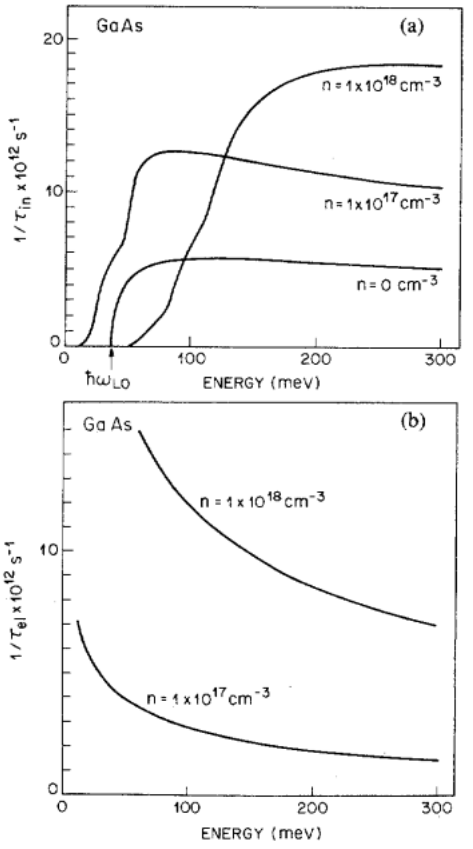

Fig. 6. (a) Total inelastic electron scattering rate as a function of injected electron energy measured from the conduction band minimum for different carrier densities in GaAs. (b) Total elastic electron scattering. Parameters used in calculations were effective electron mass $m_e^* = 0.07\ m_0$, high-frequency dielectric constant $\epsilon_\infty = 11.1$, longitudinal optical phonon energy $\hbar\omega_{LO} = 36.3$ meV, and transverse optical phonon energy $\hbar\omega_{TO} = 33.3$ meV.

$$\frac{1}{\tau_{\text{el}}} = \frac{2\pi n_i m_e^* e^4}{\hbar^3 k_i^3} \int \frac{\eta d\eta}{[\eta^2 \epsilon(2k_i\eta, 0)]^2} \tag{10}$$

where n_i is the density of ionized impurities ($n_i = n$) and $\eta \equiv \sin(\theta/2)$. In Fig. 6(b) the total elastic scattering rate $1/\tau_{\text{el}}$, which has not been weighted for scattering angle, is plotted as a function of E_i for two impurity concentrations. As expected for Coulombic scattering, $1/\tau_{\text{el}}$ decreases with increasing E_i. We cannot, however, take unlimited advantage of this decrease in the scattering rate with increasing E_i, since intervally scattering can occur in GaAs when $E_i \gtrsim 0.3$ eV. By considering both elastic and inelastic scattering we obtain a calculated mean free path for electrons injected at $E_i = 0.25$ eV of ~ 350 Å.

Our calculations of scattering rates as a function of injection energy play an important role aiding understanding of hot electron spectra. The sequence of spectra shown in Fig. 3 gives the evolution of the hot electron distribution with distance from the step potential that injected a collimated beam of almost monoenergetic hot electrons into the transit region. Sample 3(a), having the narrowest transit region width, shows two distinct features; a peak at high barrier energies (low voltage bias, V_{bc}) which we attribute to "ballistic" electrons, i.e., electrons which have only interacted with the static periodic part of the

crystal's lattice potential, and a second narrower peak in the spectrum at lower analyzer barrier energies (high V_{bc}), close to the Fermi energy, attributed to electrons excited from the Fermi sea, i.e., the electron distribution in the transit region has been "heated" by interaction with the injected electrons. Now consider Fig. 3(b) which shows results obtained from a sample having a transit region width of 850 Å. In this case the "ballistic" peak can only just be seen and most electrons have been scattered and are collected at lower barrier potentials (greater V_{bc}). Such a characteristic may be understood by considering the energy dependent scattering rate detailed in Fig. 6 since the electrons are injected with energy ~250 meV their scattering rate is very high. However, once they have lost energy such that they are only 150 meV or less above the conduction band minimum their scattering rate decreases and electrons begin to accumulate at lower energies. Fig. 3(c) shows the progression of this process by increasing the transit region width to 1200 Å. There is little evidence of the initial injected peak and a large low-energy peak which includes many electrons scattered from high energies as well as those excited from the Fermi sea. Finally, Fig. 3(d) shows a spectrum obtained from a sample with a 1700 Å transit region width in which only the low-energy peak remains, containing contributions from both the injected electrons and those excited from the Fermi sea.

We have obtained further experimental information on the dynamics of injected hot electron transport by applying a magnetic field perpendicular ($B_\perp$) to the direction of electron injection in the sample having a transit region width of 650 Å. The study was undertaken for two reasons, firstly to measure changes in a given spectrum with applied magnetic field to establish that hot electron effects were indeed being observed and secondly to infer a scattering rate for hot electrons from changes in the spectra with $B_\perp$.

The simplest description of hot electron transport utilizes a classical kinematical model in which an electron injected into the transit region, prior to the application of a magnetic field, has a straight trajectory between scattering events. However, when a magnetic field is applied this trajectory is modified, the electron describes part of a circular orbit between collisions, the radius of which r is given by

$$r = \frac{pc}{B_\perp e} \tag{11}$$

where p is the electron's momentum, e its charge, c the velocity of light, and $B_\perp$ the applied magnetic field in Gauss.

To understand the effect of the magnetic field consider what would happen to an electron transiting from the injector to the analyzer "ballistically." A nonequilibrium electron injected into the transit region with energy E_i and with all its momentum $p = \sqrt{2m_e E_i}$ in the forward direction is analyzed after traversing d the transit region width. When $B_\perp$ is applied to the sample two effects occur that

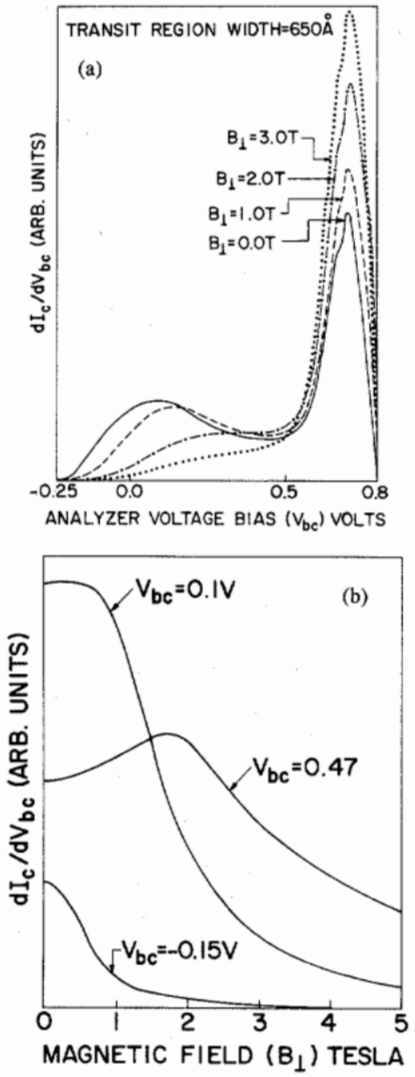

Fig. 7. (a) The variation of the hot electron spectrum shown in Fig. 3(a) for the indicated values of magnetic field applied perpendicular to the injected current. (b) The magnetic field dependence of the hot electron spectrum shown in Fig. 8(a) for the indicated values of fixed bias V_{bc}.

influence the collection of the injected electron. Firstly, the electron trajectory is increased from d to d', and hence the probability for an electron to be scattered is increased. Secondly, although the magnitude of the momentum of a "ballistic" electron remains unchanged its normal component is reduced when it reaches the analyzer because of the imposed circular orbit. The analyzer barrier, descriminating only against the normal component of momentum, collects the electron at a lower barrier energy. This qualitative description of "ballistic" electron transport in a magnetic field may be applied in a natural way to the case of hot electron transport when electrons are scattered in the transit region. The application of $B_\parallel$ should show no change in the spectra since $B_\parallel$ has no effect on the normal component of momentum.

The results of measurements at 4.2 K on a sample having a transit region width of 650 Å are shown in Fig. 7(a) for $B_\perp$ up to 3 Tesla. As may be seen in Fig. 7(a) with increasing magnetic field the high-energy "ballistic" peak at $V_{bc} \sim 0.1$ V bias shifts to larger V_{bc} (lower collector

barrier energy) resulting from the change in the component of normal momentum of electrons arriving at the analyzer. We also note that the intensity of the "ballistic" peak decreases and spectral weight is transfered to lower collector barrier energies indicating that the electrons transiting the base have suffered collisions due to the increased effective transit distance in a magnetic field. The peak at low collector barrier energies ($V_{bc} \sim 0.7$ V) broadens and increases in intensity with increasing magnetic field. Qualitatively, this is expected since both more electrons are excited from the Fermi sea and an increased number of hot electrons are inelastically scattered down to low energies. For clarity in Fig. 7(b) we plot the magnetic field dependence of the hot electron spectrum for the indicated values of V_{bc}.

It is possible to infer a hot electron scattering rate from the magnetic field dependence using two reasonable assumptions [18]. Firstly, electrons scattered due to an increase in effective transit region width (d to d') lose sufficient energy that they no longer contribute to the collected current at a given analyzer energy. Secondly, the change in the average perpendicular momentum of electrons not scattered due to the increase in the transit region width is givn by the cross product of the magnetic field and the velocity. Using these assumptions we have obtained a scattering rate for the injected electrons of 2–3×10^{13} s^{-1}. This is at least four times the rate we would expect for phonon emission alone.

It is interesting to note that application of a magnetic field of $B_\perp = 1.5$ Tesla on a sample with $d = 650$ Å allows one to reproduce the spectra of a sample having a transit region width of 850 Å with $B_\perp = 0$. However, application of a magnetic field in a direction parallel to the electron motion has no effect on the spectra. This of course is not surprising since, in this case, we expect injected electrons to follow a helical path between collisions so that the effective path length between injector and analyzer remains unchanged.

Using the theory outlined above we have interpreted our experimental data and obtained a dynamic picture of injected hot electron transport in GaAs. To gain a more quantitative measure of the agreement between experiment and theory multiple scattering events must be taken into account explicitly. Monte Carlo calculations relevant to our experimental conditions have been performed and the reported overall agreement between our experimental data and the simulations is good [19], [20]. In particular, when both the injected electrons and those excited from the Fermi sea are included in the calculation, the agreement between our published results for a sample with a 650 Å transit region width [13] and theory [20] is excellent (see Fig. 8). This agreement lends additional support for the validity and accuracy of the theory we used to interpret our measured spectra.

Both our experimental and theoretical results indicate that GaAs is an unsuitable material for the fabrication of a useful, high-performance, "ballistic" electron transistor (BET) because of the short mean free path of injected hot electrons. Regardless of the mechanism of electron injection or collection it is anticipated that device performance will be dominated by base transit dynamics. There are two approaches to consider whilst designing a BET in a material system other than GaAs/AlGaAs. One possibility is to chose a semiconductor with a wide intervalley separation in order to take advantage of the decrease in scattering rate with increasing energy. The other is to consider a material with a low effective mass and thereby lower density of states, giving a reduced electron scattering rate.

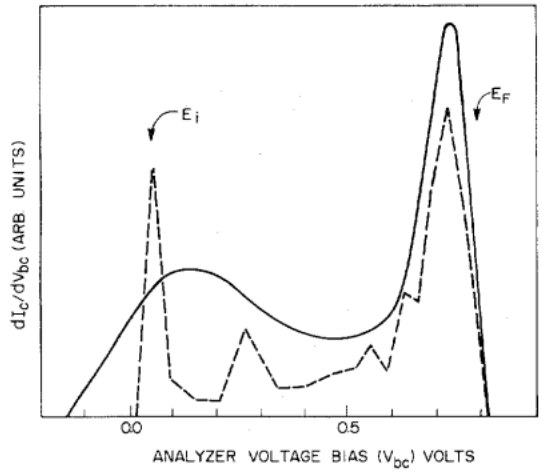

Fig. 8. Comparison of experimental data [13] (solid line) with a Monte Carlo calculation [20] (broken line). Electron injection energy $E_i = 0.25$ eV, carrier concentration $n = 1 \times 10^{18}$ cm^{-3}, and transit region width 650 Å was used in the simulation.

A semiconductor illustrating the first case could be CdTe which has a direct band gap of 1.3 eV and a subsidiary minimum 1.1 eV above the conduction band minimum. Such a material, however, with its large effective electron mass $m_e^* = 0.1m_0$ is unsuitable for "ballistic" devices. Alternatively, a semiconductor which satisfies the low mass condition would be InAs or InSb. InAs and InSb both have significantly lower inelastic scattering rates compared to GaAs. Because it may be possible to lattice match wider band gap alloys such as GaInAsSb to InAs we consider it in preference to InSb. As is the case with many low m_e^* semiconductors InAs has a small band gap energy, $E_g \sim 0.41$ eV which is less than the energy difference between the subsidiary and conduction band minimum. Consequently, whereas the maximum injection energy $E_i^{\max}$ in GaAs was determined by the subsidiary L minimum [21], for InAs $E_i^{\max}$ must satisfy $E_i^{\max} \lesssim E_g + E_F$ to avoid the possibility of direct excitation of electrons from the valence band into the conduction band: as also occurs in InSb [22].

In Fig. 9(a) and (b) we plot $1/\tau_{in}$ and $1/\tau_{el}$, respectively, for InAs as a function of E_i for various base impurity concentrations. The calculated scattering rates have features similar to those shown in Fig. 6 only now the rates for a given E_i are significantly reduced. Differences in electron mobility between InAs and GaAs mean that a BET device with an $n = 1 \times 10^{18}$ cm^{-3} doped GaAs base should be compared to a significantly lower doped InAs base. For

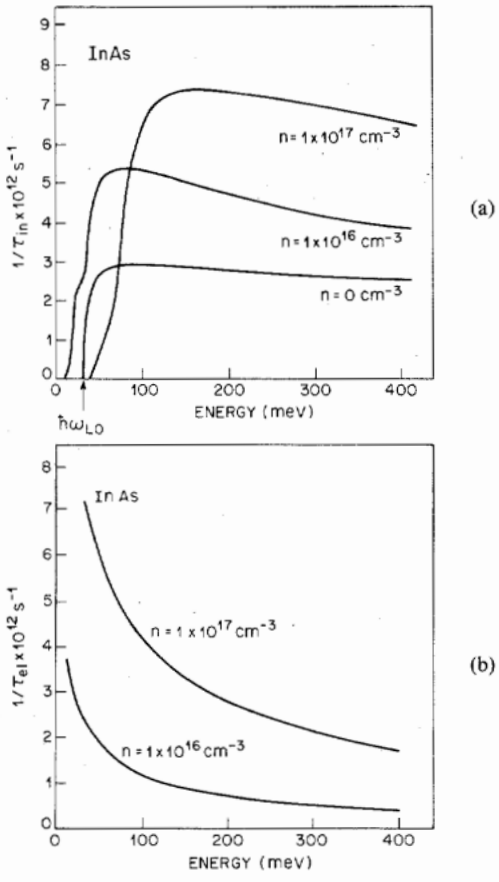

Fig. 9. (a) Total inelastic electron scattering rate as a function of injected electron energy measured from the conduction band minimum for different carrier densities in InAs. (b) Total elastic electron scattering. Parameters used in calculations were effective electron mass $m_e^* = 0.021\ m_0$, high-frequency dielectric constant $\epsilon_\infty = 11.8$, longitudinal optical phonon energy $\hbar\omega_{LO} = 30.2$ meV, and transverse optical phonon energy $\hbar\omega_{TO} = 27.1$ meV.

$n = 1 \times 10^{16}$ cm^{-3} and $E_i = 0.4$ eV electrons in InAs have a total mean free path of around 3000 Å giving, for a 500 Å base width, a "ballistic" common base current gain $\alpha_B = 0.85$. This is a promising improvement when compared to GaAs.

Irrespective of whether the semiconductor used is GaAs or InAs to improve device performance still further we are forced to consider a different means of confining thermal electrons to the base region. An obvious approach is to create a uniform (fluctuation free) potential well such as occurs in a two-dimensional electron gas at a GaAs/AlGaAs interface. In this case, elastic scattering may be reduced to a minimum by use of "modulation doping" which spatially removes the donor ions from the confined electron gas [23]. The base region will only be ~100 Å wide and inelastic electron scattering rates are reduced over those calculated for the three-dimensional case described above (because of the reduction in density of states) so that α_B could easily approach unity. In addition the high conductivity which may be achieved at low temperature leads to a significant reduction in base resistance, a very desirable feature in a high-performance transistor.

In conclusion we have designed and implemented a unique spectroscopic probe with which to study nonequilibrium electron transport in semiconductors. Our technique of hot electron spectroscopy has enabled us to establish the existence of "ballistic" electron transport together with a complete picture of the dynamics of injected electron cooling in GaAs. A full description of the measured spectra has been obtained by considering scattering from the coupled electron/phonon system, with the low-energy portion of the spectrum attributed to electrons excited from the Fermi sea. We find excellent agreement between experimental and theoretical determinations of hot electron mean free paths. It has also been shown that the short mean free paths in doped GaAs make it an unsuitable material from which to fabricate a useful hot electron transistor. We suggest InAs as a more favorable material and a two-dimensional electron gas as a more suitable means of confining electrons to the transistor base.

Acknowledgment

We wish to thank S. J. Allen, R. Bhat, A. C. Gossard, S. L. McCall, P. M. Platzmann, and H. L. Stormer for many useful discussions. We also acknowledge M. Anzlowar, T. Uchida, and W. Wiegmann for technical assistance. The continued support and encouragement of R. C. Dynes, P. F. Liao, and V. Narayanamurti is much appreciated.

References

[1] For a review of this early work see S. M. Sze, *Physics of Semiconductor Devices*. New York: Wiley, 1981.
[2] J. M. Shannon, "Hot electron camel transistor," *IEE J. Solid State Electron Devices*, vol. 3, pp. 142–144, 1979.
[3] J. M. Shannon and A. Gill, "High current gain in monolithic hot electron transistors," *Electron. Lett.*, vol. 17, pp. 620–621, 1981.
[4] R. J. Malik, T. R. AuCoin, R. L. Ross, K. Board, C. E C. Wood, and L. F. Eastman, "Planar doped barriers in GaAs by molecular beam epitaxy," *Electron. Lett.*, vol. 16, pp. 836–838, 1980.
[5] R. J. Malik, M. A. Hollis, L. F. Eastman, D. J. Woodard, C. E. C. Wood, and T. R. AuCoin, in *Proc. Conf. Active Microwave Devices*, Cornell Univ., Ithaca, NY, 1981.
[6] S. Muto, K. Imamura, N. Yokoyama, S. Hiyamizu, and H. Nishi, "Subpicosecond base transit time observed in a hot electron transistor," *Electron. Lett.*, vol. 21, pp. 555–556, 1985; J. M. Woodcock, J. J. Harris, and J. M. Shannon, "Monolithic hot electron transistor in GaAs with high current gain," *Physica*, vol. 134B, pp. 111–118, 1985; M. Heiblum, D. C. Thomas, C. M. Knoedler, and M. I. Nathan, "Tunneling hot electron transfer amplifier," *Appl. Phys. Lett.*, vol. 47, pp. 1105–1107, 1985.
[7] E. J. Ryder and W. Shockley, "Mobilities of electrons in high electric fields," *Phys. Rev.*, vol. 81, pp. 139–140, 1951.
[8] J. B. Gunn, "Microwave oscillations of current in III–V semiconductors," *Solid State Commun.*, vol. 1, pp. 88–91, 1963.
[9] J. Shah and R. C. C. Leite, "Radiative recombination from photoexcited hot carriers in GaAs," *Phys. Rev. Lett.*, vol. 22, pp. 1304–1307, 1969.
[10] J. R. Hayes, A. F. J. Levi, and W. Wiegmann, "Hot electron spectroscopy," *Electron. Lett.*, vol. 20, pp. 851–852, 1984.
[11] —, "Hot electron spectroscopy of GaAs," *Phys. Rev. Lett.*, vol. 54, pp. 1570–1572, 1985.
[12] R. F. Kazarinov and S. Luryi, "Charge injection over triangular barriers in unipolar semiconductor structures," *Appl. Phys. Lett.*, vol. 38, pp. 810–812, 1980.
[13] A. F. J. Levi, J. R. Hayes, P. M. Platzman, and W. Wiegmann, "Injected hot electron transport in GaAs," *Phys. Rev. Lett.*, vol. 55, pp. 2071–2073, 1985.
[14] M. Heiblum, M. I. Nathan, D. C. Thomas, and C. M. Knoedler, "Direct observation of ballistic electron transport in GaAs," *Phys. Rev. Lett.*, vol. 55, pp. 2200–2203, 1985.

[15] A. F. J. Levi, J. R. Hayes, P. M. Platzman, and W. Wiegmann, "Hot electron spectroscopy of GaAs," *Physica*, vol. 134B, p. 480–486, 1985.
[16] M. E. Kim, A. Das, and S. D. Senturia, "Electron scattering interaction with coupled plasmon polar phonon modes in degenerate semiconductors," *Phys. Rev.*, vol. B18, pp. 6890–6899, 1978.
[17] D. Pines and P. Nozieres, *The Theory of Quantum Liquids*. New York: Benjamin, 1966.
[18] J. R. Hayes, A. F. J. Levi, and W. Wiegmann, "Magnetic field dependence of hot electron transport in GaAs," *Appl. Phys. Lett.*, vol. 47, pp. 964–966, 1985.
[19] T. Wang, K. Hess, and G. J. Iafrate, "Monte Carlo simulations of hot electron spectroscopy in planar doped barrier transistors," *J. Appl. Phys.*, vol. 59, pp. 2125–2128, 1986.
[20] A. P. Long, P. H. Beton, and M. J. Kelly, "Hot electron transport in heavily doped GaAs," *Semiconductor Sci. Technol.*, vol. 1, pp. 63–70, 1986.
[21] J. S. Blakemore, "Semiconducting and other major properties of gallium arsenide," *J. Appl. Phys.*, vol. 53, pp. R123–181, 1982.
[22] M. Glicksman and M. C. Steele, "High field effects in n-indium antimonide," *Phys. Rev.*, vol. 110, pp. 1204–1205, 1958.
[23] R. Dingle, H. L. Störmer, A. C. Gossard, and W. Wiegmann, "Electron mobilities in modulation doped semiconductor heterojunction superlattices," *Appl. Phys. Lett.*, vol. 33, pp. 665–667, 1978.

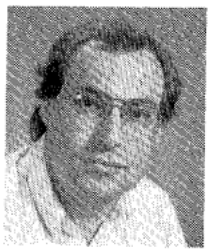

J. R. Hayes was born in London, England, on November 5, 1955. He received the B.Sc. and Ph.D. degrees in physics from the University of Surrey, Guildford, Surrey, England.

From 1982 to 1983 he was employed as a Postdoctoral Researcher at Bell Telephone Laboratories. Since 1984 he has been a member of the Technical Staff at Bell Communications Research Inc., Murray Hill, NJ.

A. F. J. Levi received the B.Sc. degree from the University of Sussex, Falmer, U.K., in 1980, and the Ph.D. degree from Cambridge University, Cambridge, U.K., in 1983.

He has been a member of the Technical Staff in the Physics Research Division at AT&T Bell Laboratories, Murray Hill, NJ, since 1984.